

Fast and spectrally accurate Ewald summation for 2-periodic electrostatic systems

Dag Lindbo^{1,*} and Anna-Karin Tornberg¹

¹*Numerical Analysis, Royal Inst. of Tech. (KTH), 100 44 Stockholm, Sweden*

September 1, 2011

Abstract

A new method for Ewald summation in planar/slabblike geometry, i.e. systems where periodicity applies in two dimensions and the last dimension is “free” (2P), is presented. We employ a spectral representation in terms of both Fourier series and integrals. This allows us to concisely derive both the 2P Ewald sum and a fast PME-type method suitable for large-scale computations. The primary results are: (i) close and illuminating connections between the 2P problem and the standard Ewald sum and associated fast methods for full periodicity; (ii) a fast, $O(N \log N)$, and spectrally accurate PME-type method for the 2P k-space Ewald sum that uses vastly less memory than traditional PME methods; (iii) errors that decouple, such that parameter selection is simplified. We give analytical and numerical results to support this.

1 Introduction

Ewald summation deals with the task of summing the Coulomb potential over a set of charged particles that are subject to periodic boundary conditions. The potential sum itself may be written as

$$\varphi(\mathbf{x}) = \sum_{n=1}^N \sum_{\mathbf{p} \in \Lambda} \frac{q_n}{\|\mathbf{x} - \mathbf{x}_n + f(\mathbf{p})\|}, \quad (1)$$

where $\{\mathbf{x}_j, q_j\}, j = 1 \dots N$, with $\mathbf{x} \in \Omega \subset \mathbb{R}^3$ and $\sum q_j = 0$ (neutrality), represents the location and charge of N particles. For simplicity we let $\Omega = [0, L]^3$. Periodicity is expressed by a translation function $f : \Lambda \rightarrow \mathbb{R}^3$, and $\Lambda = \mathbb{Z}^d$ denotes indices in a d -dimensional lattice, $d = 1, 2, 3$.

Complications, which depend on the dimension of periodicity, d , arises because the terms in (1) decay $\sim 1/r$. In fact, a certain amount of ambiguity surrounds direct summation of (1), see the appropriately named paper by Takemoto et. al. [52].

The present work deals with the accurate (spectrally) and efficient ($N \log N$) computation of the potential sum under two-dimensional periodicity (the third dimension is “free”), i.e. when $\Lambda = \mathbb{Z}^2$, and $f(\mathbf{p}) = [p_1, p_2, 0]$ (see Figure 1). We shall start by briefly surveying the fully periodic case.

*To whom correspondence should be addressed. Email: dag@kth.se

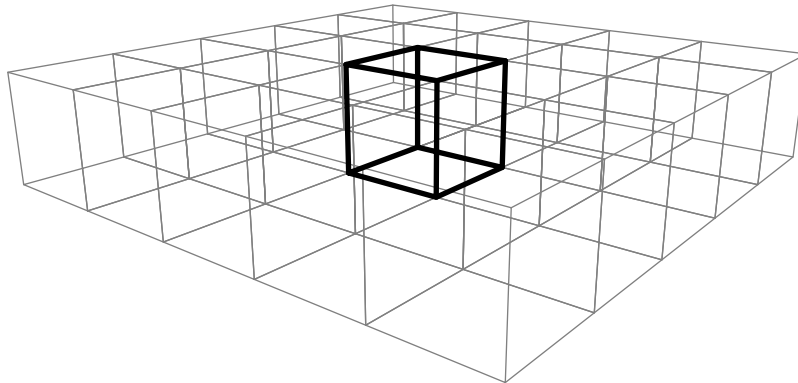


Figure 1: 2P system: Unit cell Ω (black) repeated infinitely in the plane.

1.1 3P: Fully extended periodicity

In the most common situation, periodicity is extended in all three dimensions, i.e. that $\Lambda = \mathbb{Z}^3$ and $f(\mathbf{p}) = L\mathbf{p}$. This problem has been thoroughly studied, going back to the eponymous Ewald, who in 1921 [15] showed that (1) can be computed by splitting the sum into a rapidly decaying part and a smooth part which is summed in frequency domain,

$$\varphi^{3P}(\mathbf{x}_m) = \sum_{n=1}^N \sum_{\mathbf{p}} q_n \frac{\operatorname{erfc}(\xi \|\mathbf{x}_m - \mathbf{x}_n + L\mathbf{p}\|_2)}{\|\mathbf{x}_m - \mathbf{x}_n + L\mathbf{p}\|_2} + \frac{4\pi}{L^3} \sum_{\mathbf{k}_3 \neq 0} \frac{e^{-k^2/4\xi^2}}{k^2} \sum_{n=1}^N q_n e^{-i\mathbf{k}_3 \cdot (\mathbf{x}_m - \mathbf{x}_n)} - \frac{2\xi q_m}{\sqrt{\pi}}, \quad (2)$$

where $\xi > 0$ (which φ is independent of) is known as the Ewald parameter, $\mathbf{k}_3 \in \{2\pi\mathbf{n}/L : \mathbf{n} \in \mathbb{Z}^3\}$, $k = |\mathbf{k}|$, and the term ($n = m, \mathbf{p} = 0$) is excluded from the real space sum.

The utility of Ewald summation was greatly enhanced by the development of $\mathcal{O}(N \log N)$ methods, avoiding the severely limiting $\mathcal{O}(N^2)$ complexity of evaluating (2) for all \mathbf{x}_m . We denote by *PME* (Particle Mesh Ewald) the well known family of methods that derive from the pioneering P^3M method by Hockney and Eastwood [25], including major developments such as the PME method due to Darden et. al. [7] and the SPME method by Essmann et. al. [14]. The consistency within the PME family is illustrated in the excellent surveys by Deserno and Holm [11], and Shan et. al. [49]. In a survey of electrostatic calculations in structural biology, an important application area, Koehl [33] points out that the success of Ewald's method overshadows other methods and that the applications community has flourished because of this.

1.2 2P: Planar periodicity

We shall denote the situation when periodicity applies in two dimensions and the third dimension is free as *planar periodicity* or 2P, as illustrated in Figure 1. One may think of a sheet or lamina of charges confined by $z \in [0, L]$ and infinitely replicated in the (x, y) -plane. In the literature this situation is sometimes referred to as *slab/slablike geometry* or a *quasi-two-dimensional* system and enjoys a wealth of acronyms, such as *3D2P1F* (i.e. a three-dimensional system, with two periodic directions, and one free).

As noted, a satisfactory way to sum the 3P problem came about in the 1920's and work on fast methods took off in the 1990's, based on the Ewald sum (2). In contrast, analysis and methods for the 2P problem lagged quite far behind, and fast methods have yet to reach the maturity of their 3P cousins. A summation formula analogous to (2) has emerged, but fundamentally different (i.e. non-Ewald) ideas are also being pursued.

This result, which we shall refer to as the *2P Ewald sum*, was derived by Grzybowski, Gwozdz and Brodka in [20] using lattice sums. Here, the potential sum

$$\varphi(\mathbf{x}) = \sum_{n=1}^N \sum_{\mathbf{p} \in \mathbb{Z}^2} \frac{q_n}{\|\mathbf{x} - \mathbf{x}_n + \tilde{\mathbf{p}}\|}, \quad (3)$$

with $\tilde{\mathbf{p}} = L[p_1, p_2, 0]$, is shown to equal

$$\begin{aligned} \varphi(\mathbf{x}_m) = & \sum_{n=1}^N \sum_{\mathbf{p} \in \mathbb{Z}^2}^* q_n \frac{\operatorname{erfc}(\xi|\mathbf{x}_m - \mathbf{x}_n + \tilde{\mathbf{p}}|)}{|\mathbf{x}_m - \mathbf{x}_n + \tilde{\mathbf{p}}|} + \\ & + \frac{\pi}{L^2} \sum_{n=1}^N \sum_{\mathbf{k} \neq 0} \frac{e^{i\mathbf{k} \cdot (\mathbf{r}_m - \mathbf{r}_n)}}{k} \left[e^{k(z_m - z_n)} \operatorname{erfc} \left(\frac{k}{2\xi} + \xi(z_m - z_n) \right) + \right. \\ & \left. + e^{-k(z_m - z_n)} \operatorname{erfc} \left(\frac{k}{2\xi} - \xi(z_m - z_n) \right) \right] + \\ & - \frac{2\sqrt{\pi}}{L^2} \sum_{n=1}^N q_n \left(e^{-\xi^2(z_m - z_n)^2} / \xi + \sqrt{\pi}(z_m - z_n) \operatorname{erf}(\xi(z_m - z_n)) \right) - q_m \frac{2\xi}{\sqrt{\pi}}, \quad (4) \end{aligned}$$

where $\mathbf{r} \in \mathbb{R}^2$ is the (x, y) -component of \mathbf{x} , and $\mathbf{k} \in \{2\pi\mathbf{n}/L : \mathbf{n} \in \mathbb{Z}^2\}$.

Their approach follows a classical derivation of the 3P Ewald sum by de Leeuw et. al. [10]. Interestingly, and as Grzybowski et. al. point out, the exact same expression can be obtained from much earlier work by Bertaut [4] and, more recently, by Heyes et. al. [23, 21, 24, 22]. However, it is also attributed to de Leeuw and Perram [9] by other authors (e.g. [32]). Another group with a strong claim of independently developing the 2P Ewald sum is Rhee et. al. [46]. Among the foremost in early developments was Parry [42, 43], whose results are drawn upon by Heyes and others. In the context of the present work, it is appropriate to highlight Grzybowski et. al. [20] as a modern and accessible reference. Irrespective of how one traces the lineage of (4), evaluating it for all \mathbf{x}_m has the dreaded $\mathcal{O}(N^2)$ complexity (with a *very* large constant) without hinting how a fast method might arise.

There are several alternatives to the 2P Ewald sum (4). An interesting non-Ewald method is known as *Lekner summation*, due to J. Lekner [35, 36], which obtains series that converge faster than the Ewald sum. The reader is referred to the excellent survey by Mazars [39] for more details, including comparisons between Lekner and Ewald sums, and appropriate caveats. Arnold and Holm [3] suggest a ‘‘convergence factor’’ approach – obtaining a non-Ewald method that goes by the name *MMM2D*, and is related to the Lekner sum. They, for the first time, show *a priori* error bounds for the 2P problem.

Another important alternative to (4) is, somewhat brazenly, to use the 3P Ewald sum (2) instead. The idea here is to extend the unit cell in the z -direction, creating a gap that separates sheets of charged particles (periodicity in all three directions is implied). Convergence is expected because the artificial sheets have no net charge. This was investigated by Spohr [50], where it is indicated, computationally for a simple system, that (2) converges to (4) as

the gap widens. Various methods have been proposed that introduce correction terms to the 3P sum, such as the method due to Yeh and Berkowitz [54] (see also Crozier et. al. [6]). Present in these references (and in the works cited therein) are, to a varying extent, additional assumptions and physically motivated simplifications that do not immediately generalize. The level of accuracy attained by these methods is seen as inadequate by present standards.

Moreover, the errors introduced by extending the problem to 3D periodicity turn out to be quite subtle. In a pair of papers [2, 8], Arnold, Holm and de Joannis show that by formally summing in a planar fashion (rather than spherically, as is implied in the Ewald sum (2)) additional terms emerge. This lets them formulate a correction term which enables high accuracy and good error control when used in conjunction with their MMM2D method [3]. They also apply established PME methods to the extended problem, obtaining a fast method. The work by Holm et. al. deserves much credit for clarity, appropriate rigor, and a level of general applicability which is lacking in much of the preceding work.

There also exists methods that aim to improve the efficiency of evaluating the 2P Ewald sum (4). In a collection of papers Kawata and collaborators [29, 28, 30] propose a method which relies on an integral transform that was also used by Parry [42, 43] (see clarifying correspondence [38, 31]). The same authors have also proposed a SPME-like method [32] that relies on the same ideas. However, even the determined reader may struggle to gain clarity from these sources – and the practical accuracy of their methods appears to be low and hard to control. This is regrettable, as we believe that their basic premises are quite useful. This shall be elaborated on throughout the present work.

Recent work includes Ewald-related methods due to S. Goedecker and collaborators, such as the mixed Ewald-finite element method by Ghasemi et. al. [18] and related work [17, 41].

Of the available methods, the work by Holm et. al. appears to be the one most widely used. This might well be a consequence of their proximity to established 3P methods – which would explain why other recent work enjoys less attention. For instance, the idea that Ghasemi et. al. pursue [18] (using a tailored finite element method in the z -direction) adds significantly to the mathematical and practical complexity of the problem at hand *vis-a-vis* 3P methods.

We agree with the view promoted by Holm et. al., that there is much value in having methods for the 2P problem that maintain a close relationship to the mature 3P methods. However, we believe that extending the problem to full periodicity, and then laboring extensively over correction terms to compensate, is a somewhat blunt approach.

In the present work, we shall use a more subtle approach that avoids the extension to full periodicity, yet is consistent with the 3P Ewald framework. It starts from representing functions with planar periodicity (2P) using both Fourier series (in the periodic (x, y) -directions) and a Fourier integral (in the free z -direction). We show that this admits a natural derivation of the 2P Ewald sum (4). Furthermore, we shall see that an intermediate step in this derivation is a natural starting point from which a fast, $\mathcal{O}(N \log N)$, and spectrally accurate method can be developed. We derive this method and motivate it theoretically and with computational examples.

2 Ewald summation in planar periodicity

2.1 Preliminaries

Start by defining a set of functions of mixed periodicity (2D periodic 1D free).

Definition 2.1 (2P functions). *Let V_Ω denote the set of functions $f(x, y, z)$ that are periodic in $(x, y) \in \Omega$ and “free” in $z \in \mathbb{R}$. Denote $V_\Omega \ni f(\mathbf{r}, z)$, $\mathbf{r} = (x, y) \in \Omega$. We shall refer to these as functions of mixed periodicity. Functions in V_Ω have a discrete spectrum corresponding to the periodic directions, and a continuous spectrum corresponding to z . We let $V_\Omega \ni f(\mathbf{r}, z) = \hat{f}(\mathbf{k}, \kappa)$, $\mathbf{k} \in \{2\pi\mathbf{n}/L : \mathbf{n} \in \mathbb{Z}^2\}$, $\kappa \in \mathbb{R}$.*

We assume that $f(\mathbf{r}, z)$ and all its derivatives decay faster than any inverse power of z in the limit $|z| \rightarrow \infty$, and that $\int_\Omega |f(\mathbf{r}, z)|^2 d\mathbf{r} < \infty$ for all z . Then \hat{f} exists and represents $f \in V_\Omega$ (with $\Omega = [0, L]^2$):

$$f(\mathbf{r}, z) = \frac{1}{2\pi} \int_{\mathbb{R}} \sum_{\mathbf{k}} \hat{f}(\mathbf{k}, \kappa) e^{i\mathbf{k}\cdot\mathbf{r}} e^{i\kappa z} d\kappa. \quad (5)$$

In fact, in the present work we mostly deal with Gaussians, $e^{-\alpha r^2}$, i.e. the fixed point of the Fourier transform (a Schwartz function). As far as spectral properties are concerned, this is a very strong setting.

We shall need several fundamental results from Fourier analysis, including Poisson summation, Parseval/Plancherel’s formula and the convolution theorem. Typically, these results are given for either free-space or periodic functions, see e.g. Pinsky [44, Ch. 4] and Vretblad [53, pp. 175-181]. For functions in V_Ω we have the following:

Lemma 2.1 (Poisson summation). *Let $f(\mathbf{x}) \in V_\Omega$ have Fourier transform \hat{f} , and let $L \neq 0$. Then,*

$$\sum_{\mathbf{p} \in \mathbb{Z}^2} f(\mathbf{x} + \tilde{\mathbf{p}}) = \frac{1}{2\pi L^2} \int_{\mathbb{R}} \sum_{\mathbf{k}} \hat{f}(\mathbf{k}, \kappa) e^{i\mathbf{k}\cdot\mathbf{r}} e^{i\kappa z} d\kappa,$$

where $\tilde{\mathbf{p}} = [L\mathbf{p}, 0]$ and $\mathbf{x} =: (\mathbf{r}, z)$.

Lemma 2.2 (Parseval/Plancherel). *Let $f(\mathbf{x}) \in V_\Omega$ have Fourier transform \hat{f} . Then,*

$$\int_{\mathbb{R}} \int_{\Omega} |f(\mathbf{r}, z)|^2 d\mathbf{r} dz = \frac{1}{2\pi} \int_{\mathbb{R}} \sum_{\mathbf{k}} |\hat{f}(\mathbf{k}, \kappa)|^2 d\kappa.$$

Lemma 2.3 (Parseval/Plancherel variant). *Let $f(\mathbf{x}), g(\mathbf{x}) \in V_\Omega$ have Fourier transform \hat{f} and \hat{g} respectively. Then,*

$$\int_{\mathbb{R}} \int_{\Omega} f(\mathbf{r}, z) \overline{g(\mathbf{r}, z)} d\mathbf{r} dz = \frac{1}{2\pi} \int_{\mathbb{R}} \sum_{\mathbf{k}} \hat{f}(\mathbf{k}, \kappa) \overline{\hat{g}(\mathbf{k}, \kappa)} d\kappa.$$

Lemma 2.4 (Convolution). *The convolution of $f(\mathbf{x}), g(\mathbf{x}) \in V_\Omega$ is defined as*

$$(f * g)(\mathbf{r}, z) = \int_{\mathbb{R}} \int_{\Omega} f(\mathbf{r} - \mathbf{r}', z - z') g(\mathbf{r}', z') d\mathbf{r}' dz',$$

and satisfies

$$h(\mathbf{r}, z) = (f * g)(\mathbf{r}, z) \iff \hat{h}(\mathbf{k}, \kappa) = \hat{f}(\mathbf{k}, \kappa) \hat{g}(\mathbf{k}, \kappa).$$

2.2 Deriving the 2P Ewald sum

From these definitions and properties we now derive the 2P Ewald sum (4) in a way that naturally sets the stage for our PME-type method (Section 3). The objective is to compute

$$\varphi(\mathbf{x}) = \sum_{\mathbf{p} \in \mathbb{Z}^2} \sum_{n=1}^N \frac{q_n}{\|\mathbf{x} - \mathbf{x}_n + \tilde{\mathbf{p}}\|},$$

where $\tilde{\mathbf{p}} = L[\mathbf{p}, 0]$, $\mathbf{p} \in \mathbb{Z}^2$. The traditional way to derive the (3P) Ewald sum is to solve the Poisson problem,

$$-\Delta\varphi(\mathbf{x}) = 4\pi \sum_{n=1}^N \rho^n(\mathbf{x}), \quad \rho^n(\mathbf{x}) = \sum_{\mathbf{p} \in \mathbb{Z}^2} q_n \delta(\mathbf{x} - \mathbf{x}_n + \tilde{\mathbf{p}})$$

by introducing a charge screening function, $\gamma(\xi, \mathbf{x})$,

$$\rho^n(\mathbf{x}) = \underbrace{\rho^n(\mathbf{x}) - (\rho^n * \gamma)(\mathbf{x})}_{:=\rho^{n,R}(\mathbf{x})} + \underbrace{(\rho^n * \gamma)(\mathbf{x})}_{:=\rho^{n,F}(\mathbf{x})}. \quad (6)$$

One then builds φ from

$$\varphi = \sum_{n=1}^N (\varphi^{n,R} + \varphi^{n,F}) \quad (7)$$

after solving

$$\underbrace{-\Delta\varphi^{n,R}(\mathbf{x}) = 4\pi\rho^{n,R}(\mathbf{x})}_{(a)} \quad \text{and} \quad \underbrace{-\Delta\varphi^{n,F}(\mathbf{x}) = 4\pi\rho^{n,F}(\mathbf{x})}_{(b)}.$$

The screening function, γ , is required to go from $\gamma(\xi, 0) = 1$ to $\gamma(\xi, \|\mathbf{x}\| \rightarrow \infty) = 0$ with sufficient regularity and be normalized $\|\gamma(\xi, \mathbf{x})\|_{L^2} = 1$. The most common choice is a Gaussian,

$$\gamma(\mathbf{x}) = \xi^3 \pi^{-3/2} e^{-\xi^2 \|\mathbf{x}\|^2} \quad \Longleftrightarrow \quad \hat{\gamma}(\mathbf{k}) = e^{-k^2/4\xi^2}, \quad (8)$$

and the classical Ewald summation result follows from this. Utilizing this screening function also in the 2P setting, it's a straight forward computation to solve (a), as it is essentially the same as in 3P. One arrives at:

$$\varphi^{n,R}(\mathbf{x}) = \sum_{\mathbf{p} \in \mathbb{Z}^2} q_n \frac{\text{erfc}(\xi \|\mathbf{x} - \mathbf{x}_n + \tilde{\mathbf{p}}\|)}{\|\mathbf{x} - \mathbf{x}_n + \tilde{\mathbf{p}}\|}, \quad \mathbf{x} \neq \mathbf{x}_n.$$

In the limit $\mathbf{x} \rightarrow \mathbf{x}_n$ we wish to remove the self-interaction, which, under the screening, γ , has partly been incorporated into (b),

$$\lim_{\|\mathbf{x}\| \rightarrow 0} \left(\frac{\text{erfc}(\xi \|\mathbf{x}\|)}{\|\mathbf{x}\|} - \frac{1}{\|\mathbf{x}\|} \right) = \lim_{\|\mathbf{x}\| \rightarrow 0} -\frac{\text{erf}(\xi \|\mathbf{x}\|)}{\|\mathbf{x}\|} = -\frac{2\xi}{\sqrt{\pi}}.$$

Summing, in light of (7), gives $\sum_{n=1}^N \varphi^{n,R}(\mathbf{x}_m) = \varphi^R(\mathbf{x}_m) + \varphi^S(\mathbf{x}_m)$, with

$$\begin{aligned}\varphi^R(\mathbf{x}_m) &= \varphi_m^R = \sum_{n=1}^N \sum_{\mathbf{p} \in \mathbb{Z}^2}^* q_n \frac{\operatorname{erfc}(\xi \|\mathbf{x}_m - \mathbf{x}_n + \tilde{\mathbf{p}}\|)}{\|\mathbf{x}_m - \mathbf{x}_n + \tilde{\mathbf{p}}\|} \\ \varphi_m^S &= -q_m \frac{2\xi}{\sqrt{\pi}},\end{aligned}$$

where $*$ denotes that the term $\mathbf{p} = 0$ is excluded when $n = m$. The last term, φ^S , is usually referred to as *self interaction*.

The second equation (b) is also treated along the lines of the classical derivation of the 3P Ewald sum, though mixed periodicity will play a bigger role here. Additionally, physically motivated conditions as $z \rightarrow \pm\infty$, consistent with the charge distribution, have to be satisfied. Returning to (5), let

$$\varphi^{n,F}(\mathbf{r}, z) = \frac{1}{2\pi} \int_{\mathbb{R}} \sum_{\mathbf{k}} \hat{\varphi}^{n,F}(\mathbf{k}, \kappa) e^{i\mathbf{k} \cdot (\mathbf{r} - \mathbf{r}_n)} e^{i\kappa(z - z_n)} d\kappa.$$

Differentiation gives that

$$-\Delta \varphi^{n,F} = \frac{1}{2\pi} \int_{\mathbb{R}} \sum_{\mathbf{k}} (k^2 + \kappa^2) \hat{\varphi}^{n,F}(\mathbf{k}, \kappa) e^{i\mathbf{k} \cdot \mathbf{r}} e^{i\kappa z} d\kappa. \quad (9)$$

On the other hand, using Poisson summation (Lemma 2.1) we get

$$\begin{aligned}4\pi \rho^{n,F} &= 4\pi \sum_{\mathbf{p} \in \mathbb{Z}^2} q_n \gamma(\mathbf{x} - \mathbf{x}_n + \tilde{\mathbf{p}}) = \frac{2q_n}{L^2} \int_{\mathbb{R}} \sum_{\mathbf{k}} \hat{\gamma}(\mathbf{k}, \kappa) e^{i\mathbf{k} \cdot (\mathbf{r} - \mathbf{r}_n)} e^{i\kappa(z - z_n)} d\kappa \\ &= \frac{2q_n}{L^2} \int_{\mathbb{R}} \sum_{\mathbf{k}} e^{-(k^2 + \kappa^2)/4\xi^2} e^{i\mathbf{k} \cdot (\mathbf{r} - \mathbf{r}_n)} e^{i\kappa(z - z_n)} d\kappa.\end{aligned} \quad (10)$$

Equating (9) and (10) gives, for $k^2 + \kappa^2 > 0$,

$$\hat{\varphi}^{n,F} = \frac{4\pi q_n}{L^2} \frac{e^{-(k^2 + \kappa^2)/4\xi^2}}{k^2 + \kappa^2},$$

so that

$$\varphi^{n,F}(\mathbf{r}, z) = \frac{2q_n}{L^2} \int_{\mathbb{R}} \sum_{\mathbf{k} \neq 0} \frac{e^{-(k^2 + \kappa^2)/4\xi^2}}{k^2 + \kappa^2} e^{i\mathbf{k} \cdot (\mathbf{r} - \mathbf{r}_n)} e^{i\kappa(z - z_n)} d\kappa + \varphi^{n,F, \mathbf{k}=0}.$$

Up to this point the 2P Ewald derivation has deviated from the traditional 3P derivation only in the representation formula (5). However, there remains to discuss the $\mathbf{k} = 0$ term. We write

$$\varphi^F(\mathbf{x}_m) = \frac{2}{L^2} \sum_{n=1}^N \sum_{\mathbf{k} \neq 0} \int_{\mathbb{R}} q_n \frac{e^{-(k^2 + \kappa^2)/4\xi^2}}{k^2 + \kappa^2} e^{i\mathbf{k} \cdot (\mathbf{r}_m - \mathbf{r}_n)} e^{i\kappa(z_m - z_n)} d\kappa, \quad (11)$$

so that $\sum_{n=1}^N \varphi^{n,F}(\mathbf{r}_m, z_m) = \varphi^F(\mathbf{r}_m, z_m) + \varphi^{F, \mathbf{k}=0}$.

Before determining the term $\varphi^{F,\mathbf{k}=0}$, one can proceed further with the integral in (11). Using Erdélyi (ed.) [13, Ch. 1.4, (15), p. 15], or more the more recent Zwillinger (ed.) [55, 3.954 (2), p. 504], it follows that

$$\varphi^F(\mathbf{x}_m) = \frac{\pi}{L^2} \sum_{n=1}^N \sum_{\mathbf{k} \neq 0} \frac{e^{i\mathbf{k} \cdot (\mathbf{r}_m - \mathbf{r}_n)}}{k} \left[e^{k(z_m - z_n)} \operatorname{erfc} \left(\frac{k}{2\xi} + \xi(z_m - z_n) \right) + e^{-k(z_m - z_n)} \operatorname{erfc} \left(\frac{k}{2\xi} - \xi(z_m - z_n) \right) \right].$$

Turning to the 2P-specific contribution denoted $\varphi_m^{F,\mathbf{k}=0}$ – in the 3P Ewald sum (2), the (single) term $\mathbf{k}_3 = 0$ is simply dropped due to the condition that φ integrates to zero, which is consistent with the charge neutrality constraint, $\sum_{n=1}^N q_n = 0$. In the 2-periodic setting the relevant condition takes the form of a dipole moment with respect to z , the non-periodic direction,

$$\lim_{z \rightarrow \pm\infty} \varphi(\mathbf{x}) = \pm \frac{2\pi}{L^2} \sum_{n=1}^N q_n z_n.$$

The derivation is found in Appendix A, where the remaining contribution is found to be:

$$\varphi_m^{F,\mathbf{k}=0} = -\frac{2\sqrt{\pi}}{L^2} \sum_{n=1}^N q_n \left(\frac{1}{\xi} e^{-\xi^2(z_m - z_n)^2} + \sqrt{\pi}(z_m - z_n) \operatorname{erf}(\xi(z_m - z_n)) \right).$$

We now have all the terms present in (4) and the derivation is complete. To summarize, φ is computed from

$$\varphi(\mathbf{x}_m) = \varphi_m^R + \varphi_m^F + \varphi_m^{F,\mathbf{k}=0} + \varphi_m^S,$$

where

$$\varphi_m^R = \varphi_m^R = \sum_{n=1}^N \sum_{\mathbf{p} \in \mathbb{Z}^2}^* q_n \frac{\operatorname{erfc}(\xi|\mathbf{x}_m - \mathbf{x}_n + \tilde{\mathbf{p}}|)}{|\mathbf{x}_m - \mathbf{x}_n + \tilde{\mathbf{p}}|} \quad (12)$$

$$\varphi_m^F = \frac{2}{L^2} \sum_{n=1}^N \sum_{\mathbf{k} \neq 0} \int_{\mathbb{R}} q_n \frac{e^{-(k^2 + \kappa^2)/4\xi^2}}{k^2 + \kappa^2} e^{i\mathbf{k} \cdot (\mathbf{r}_m - \mathbf{r}_n)/L} e^{i\kappa(z_m - z_n)} d\kappa, \quad \text{or as a sum,} \quad (13)$$

$$= \frac{\pi}{L^2} \sum_{n=1}^N \sum_{\mathbf{k} \neq 0} \frac{e^{i\mathbf{k} \cdot (\mathbf{r}_m - \mathbf{r}_n)}}{k} \left[e^{k(z_m - z_n)} \operatorname{erfc} \left(\frac{k}{2\xi} + \xi(z_m - z_n) \right) + e^{-k(z_m - z_n)} \operatorname{erfc} \left(\frac{k}{2\xi} - \xi(z_m - z_n) \right) \right] \quad (14)$$

$$\varphi_m^{F,\mathbf{k}=0} = -\frac{2\sqrt{\pi}}{L^2} \sum_{n=1}^N q_n \left(e^{-\xi^2(z_m - z_n)^2} / \xi + \sqrt{\pi}(z_m - z_n) \operatorname{erf}(\xi(z_m - z_n)) \right) \quad (15)$$

$$\varphi_m^S = -q_m \frac{2\xi}{\sqrt{\pi}}. \quad (16)$$

We shall refer to (12) as the *2P real space Ewald sum*, to (14) as the *2P k-space Ewald sum*. As we have already pointed out, these expressions have been derived before, e.g. by

Grzybowski et. al. [20]. However, they arrive at (14) in a completely different manner. For us, the integral representation of φ^F (13) is the key result that we shall derive a fast and accurate PME-type method from. Kawata and Mikami [28] view (13) as a consequence of (14), which is of course valid (the expressions are equivalent), but runs counter to intuition. The theoretical foundations set forth in Section 2.1 not only enable our elementary derivation of (12)-(16) and the important choice (13) \vee (14), but are also required as we proceed.

As is well established for the 3P Ewald sum, the infinite sums above may be truncated (which we elaborate on in Section 3.5.3). Evaluating (12) or (14) $\forall m \in \{1, 2, \dots, N\}$ has complexity $\mathcal{O}(N^2)$ with a *very* large constant (that grows geometrically as higher accuracy is required). The contribution from the $\mathbf{k} = 0$ singularity (15) has the same complexity, but with a smaller constant.

3 Spectrally accurate fast method for the 2P Ewald sum

Here we develop a PME-like method with spectral accuracy to compute the reciprocal space 2P Ewald sums φ^F (14) and $\varphi^{F, \mathbf{k}=0}$ (15). The treatment is self-contained, but the reader may benefit from being familiar with our previous paper [37] on the 3P problem.

3.1 Fast method for φ^F

Consider the computation of the integral form of the 2P \mathbf{k} -space Ewald sum (13):

$$\varphi^F(\mathbf{x}_m) = \frac{2}{L^2} \sum_{\mathbf{k} \neq 0} \int_{\mathbb{R}} \frac{e^{-(k^2 + \kappa^2)/4\xi^2}}{k^2 + \kappa^2} \sum_{n=1}^N q_n e^{i\mathbf{k} \cdot (\mathbf{r}_n - \mathbf{r}_m)} e^{i\kappa(z_n - z_m)} d\kappa.$$

We proceed as in [37], splitting the Gaussian term above into three parts using a parameter $\eta > 0$ (cf. Section 3.1.1),

$$\varphi^F(\mathbf{r}_m, z_m) = \frac{2}{L^2} \sum_{\mathbf{k} \neq 0} \int_{\mathbb{R}} \frac{e^{-(1-\eta)(k^2 + \kappa^2)/4\xi^2}}{k^2 + \kappa^2} e^{-i\mathbf{k} \cdot \mathbf{r}_m} e^{-i\kappa z_m} e^{-\eta(k^2 + \kappa^2)/8\xi^2} \widehat{H}(\mathbf{k}, \kappa) d\kappa,$$

where we have let

$$\widehat{H}(\mathbf{k}, \kappa) := \sum_{n=1}^N q_n e^{-\eta(k^2 + \kappa^2)/8\xi^2} e^{-i\mathbf{k} \cdot \mathbf{r}_n} e^{-i\kappa z_n}.$$

Using the convolution theorem (Lemma 2.4) and known transforms one finds

$$H(\mathbf{r}, z) = C \sum_{n=1}^N q_n e^{-\beta \|\mathbf{r} - \mathbf{r}_n\|_*^2} e^{-\beta(z - z_n)^2}, \quad C = (2\xi^2/\pi\eta)^{3/2}, \beta = 2\xi^2/\eta, \quad (17)$$

where $\|\cdot\|_*$ denotes that periodicity is implied (in the (x, y) -plane, *nota bene*). This expression can be efficiently evaluated on a grid, but to obtain $\widehat{H}(\mathbf{k}, \kappa)$ on a suitable grid in \mathbf{k} -space we must be careful. The computation in the periodic directions is simple – just take the FFT – but in the z -direction one needs to compute the Fourier integral. We refer to this operation as a *mixed Fourier transform*, MFT(\cdot), i.e.

$$\widehat{H}(\mathbf{k}, \kappa) = \text{MFT}(H(\mathbf{r}, z)), \quad (18)$$

and clarify this in Section 3.2. Moving on, let

$$\widehat{H}(\mathbf{k}, \kappa) := \frac{e^{-(1-\eta)(k^2+\kappa^2)/4\xi^2}}{(k^2 + \kappa^2)} \widehat{H}(\mathbf{k}, \kappa), \quad (19)$$

so that

$$\varphi^F(\mathbf{r}_m, z_m) = \frac{2}{L^2} \sum_{\mathbf{k} \neq 0} \int_{\mathbb{R}} e^{-i\mathbf{k} \cdot \mathbf{r}_m} e^{-i\kappa z_m} e^{-\eta(k^2+\kappa^2)/8\xi^2} \overline{\widehat{H}(\mathbf{k}, \kappa)} d\kappa. \quad (20)$$

To proceed we use Plancherel's Theorem (Lemma 2.3) with

$$\widehat{f}(\mathbf{k}, \kappa) = e^{-i\mathbf{k} \cdot \mathbf{r}_m} e^{-i\kappa z_m} e^{-\eta(k^2+\kappa^2)/8\xi^2},$$

and $\widehat{g} = \widehat{H}(\mathbf{k}, \kappa)$. Noting that f is a \mathbf{k} -space product between Gaussians and complex exponentials, one may compute its inversion, $f(\mathbf{r}, z)$, as a convolution with δ -functions. Thus, invoking Lemma 2.4 and known transforms gives that

$$\begin{aligned} \varphi(\mathbf{x}_m) &= \frac{4\pi}{L^2} \int_{\mathbb{R}} \int_{\Omega} \widetilde{H}(\mathbf{r}, z) \left[C \int_{\mathbb{R}} \int_{\Omega} \delta(\mathbf{r}' - \mathbf{r}_m) \delta(z' - z_m) e^{-\beta \|\mathbf{r}' - \mathbf{r}_m\|_*^2} e^{-\beta(z' - z_m)^2} d\mathbf{r}' dz' \right] d\mathbf{r} dz \\ &= \frac{4\pi}{L^2} \int_{\mathbb{R}} \int_{\Omega} \widetilde{H}(\mathbf{r}, z) C e^{-\beta \|\mathbf{r} - \mathbf{r}_m\|_*^2} e^{-\beta(z - z_m)^2} d\mathbf{r} dz. \end{aligned} \quad (21)$$

Again, $\widehat{H}(\mathbf{k}, \kappa) \rightarrow \widetilde{H}(\mathbf{r}, z)$ on a grid in real space requires a non-trivial mixed transform (again, see Section 3.2), i.e. $\widetilde{H}(\mathbf{r}, z) = \text{MFT}^{-1}(\widehat{H}(\mathbf{k}, \kappa))$. The integral (21) is evaluated using trapezoidal quadrature (to spectral accuracy). In contrast to other PME-type methods, the final result (21) is an equality – no approximations have yet been introduced. Naturally, as the integral is evaluated via quadrature, and a finite grid for \mathbf{x} is employed, approximations will enter. We shall see that these errors are well controlled.

To summarize, the algorithm is: (i) compute (17), (ii) take the mixed transform (18), (iii) compute (19), (iv) take the mixed inverse transform, and finally (v) compute (21) at all desired points \mathbf{x}_m .

The key point that we wish to convey with the derivations of Sections 2.2 and 3.1 is *the minimal deviation from the treatment of 3P Ewald methods*. In particular, the fast method presented here is equivalent to established 3P PME methods with the following exceptions: Gaussians (rather than e.g. Cardinal B-splines) are used in the charge assignment step (17); an integral is evaluated (rather than interpolation) to get point-values back, in (21); and a Fourier integral replaces the DFT in the z -direction of the transforms.

3.1.1 Parameterization and modus operandi

There is a free parameter, η , that can be used to control the shape of the Gaussian used for the convolutions in (17) and (21). We find (cf. [37]) that a natural choice is to let

$$\eta = \left(\frac{2w\xi}{m} \right)^2, \quad (22)$$

where w represents the half width of a Gaussian and m its shape – see Figure 2. Let the domain $\Omega = [0, L]^3$ be discretized with M points in each direction and let $h = L/M$ denote

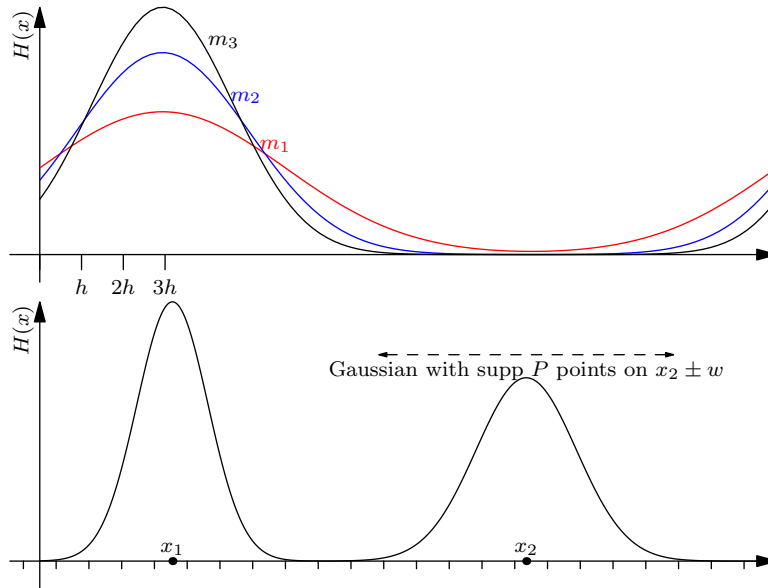


Figure 2: Top: Gaussians with different shape parameters, $m_1 < m_2 < m_3$. Bottom: Gaussian with support on P grid points around \mathbf{x}_j

the grid size. It is implied throughout that L and M can be different in each direction, and subscripts will be used when necessary, i.e. L_z and M_z .

Gaussians lack compact support, but they are highly localized. It is natural to truncate them, as is done in the non-uniform FFT [19, 12]. We let $P \leq M$ denote the number of grid points within the support of each Gaussian, as seen in Figure 2 (bottom). This naturally implies that we take $w = hP/2$. Furthermore, our analysis shows (cf. Section 3.5) that the shape parameter, m , can be chosen as $m \sim \sqrt{P}$. This leaves us with a single parameter, P .

Remark 3.1. *In contrast to traditional PME methods, we consider the grid size, M , fixed (determined by the truncation estimates of the Ewald sum). The approximation errors added by the fast method are controlled by increasing P , the number of points within the support of each Gaussian.*

3.2 Computation of Fourier integrals via FFT

We now make important clarifications regarding the non-trivial mixed transforms present in the fast method above. Recall that we have two transforms to compute: (i) from the gridded charge distribution $H(\mathbf{r}, z)$ to $\hat{H}(\mathbf{k}, \kappa)$, and (ii) from $\hat{H}(\mathbf{k}, \kappa)$ to the real-space function $\tilde{H}(\mathbf{r}, z)$. Again, $H \in V_\Omega$, and we think of this mixed periodicity in the following way: $H(\mathbf{r}, z)$ is periodic in $\mathbf{r} = (x, y)$ and free in z – hence, H has a transform, $\hat{H}(\mathbf{k}, \kappa)$, where \mathbf{k} is discrete in the sense that $\mathbf{k} \in 2\pi\mathbb{Z}^2/L$, and $\kappa \in \mathbb{R}$ is a continuous transform variable corresponding to the non-periodic dimension.

Remark 3.2. *Regardless of how these transforms are computed in practice, it is important to remember the underlying mathematics: a 2D discrete Fourier transform in (x, y) , together with a Fourier integral transform in z . The discrete transforms are, of course, computed accurately via the FFT, whereas the integral transform raises the specter of very large numerical errors. This is one of the defining differences between Ewald methods in 2P and 3P.*

Furthermore, we require that the integral transforms can be computed in the same, $\mathcal{O}(M_z \log M_z)$, complexity as the corresponding DFT in the 3P method, so as to stay relevant for large-scale calculations.

We now outline how this is done, based on remarks by Press et. al. [45, pp. 692-693]. Let $f(x) \in C^\infty$ decay sufficiently fast in the the interval (a, b) that it's Fourier integral transform can be truncated

$$\hat{f}_{a,b}(k) := \int_a^b f(x) \exp(ikx) dx, \quad |\hat{f}(k) - \hat{f}_{a,b}(k)| < \varepsilon, \quad (23)$$

for some small ε . Discretize the interval in real space with M subintervals of size $h = (b - a)/M$. We approximate the integral in a midpoint fashion,

$$\begin{aligned} \hat{f}_{a,b}(k) &\approx T_M(k) := h \sum_{j=1}^M f(x_j) \exp(ikx_j), \quad \text{with } x_j = h(j - 1) + a + h/2 = hj + a - h/2, \\ &= h \exp(ik(a - h/2)) \sum_{j=1}^M f(x_j) \exp(ikhj). \end{aligned} \quad (24)$$

Suppose we want to evaluate $\hat{f}(k)$ on a reciprocal grid $\frac{2\pi}{L}\{-M/2, \dots, M/2\} \ni k$. Then the remaining sum can be identified with the discrete Fourier transform, so that $\hat{f}(k)$ is obtained *on the entire reciprocal grid by a single FFT*.

The task of computing Fourier integral transforms numerically is well studied in a broader context – for instance there are the famous *Filon-type quadratures* (named after L. N. G. Filon who worked on predecessors to current methods in the 1920's [16]). A modern starting point is Iserles and Nørsett [26, 27], where *matched asymptotic expansions* are used to formulate accurate numerical methods for highly oscillatory integrals. They aim to compute $\hat{f}_{a,b}(k)$ for a single (very large) k with relatively few evaluations of f , under much weaker assumptions on f than we have here. For the present calculations, we may view the integral as *moderately* oscillatory. By this we mean that f falls off fast enough that the maximal characteristic frequency, $(b - a)k_1 \sim M$, of interest is modest even for very high accuracies (as shall become clear soon). Furthermore, we need to compute the Fourier integral on all points k on a reciprocal space grid, and Iserles [26, p. 367] indicates that an FFT-based method is the appropriate choice (cf. earlier work by Narasimhan [40]).

That said, we return to the midpoint quadrature (24). Press et. al. offer appropriate caution over this quadrature method: Again, the integral (23) is oscillatory for large k , and, since the maximal k is proportional to M , it is not obvious in what sense T_M converges to $\hat{f}_{a,b}(k)$ as M grows. Of course, the corresponding inverse Fourier transform may be treated similarly, and the same caution applies. To investigate the numerical errors involved we now consider two carefully chosen 1D integrals.

3.2.1 Fourier integral transform of Gaussian via FFT

In light of the computations relevant to the present work, we first restrict ourselves to a Gaussian and its transform,

$$f(x) = \exp(-\beta^2(x - x')) \quad \Leftrightarrow \quad \hat{f}(k) = \sqrt{\pi/\beta^2} \exp(-k^2/(4\beta^2)) \exp(-ikx'). \quad (25)$$

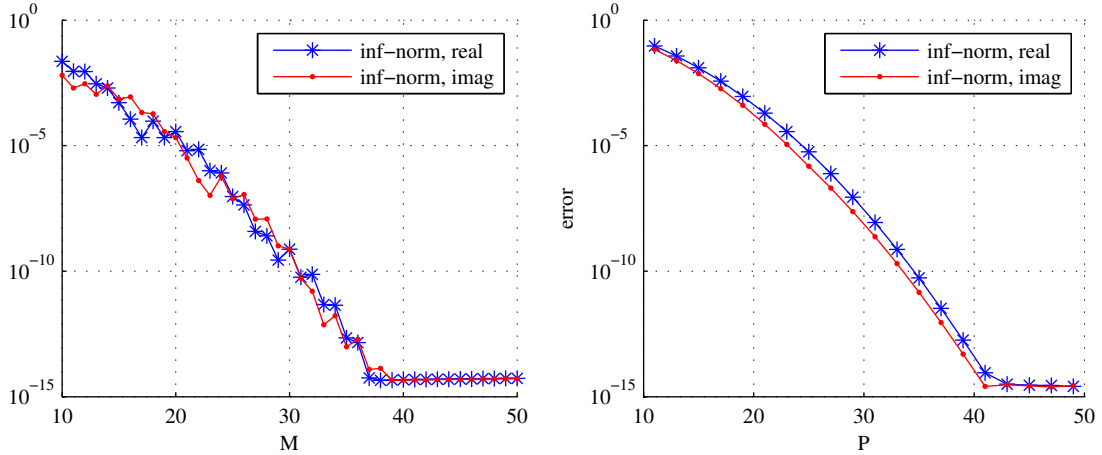


Figure 3: Left: Convergence of quadrature method (24) for computing Fourier transform of Gaussian in 1D (25). Parameters, $\beta = 9$, $x' = 0.51$, $a = -0.1$, $b = 1.1$, chosen to avoid the symmetric cases when accuracy comes easier. Right: In the *modus operandi* of the proposed method – convergence of quadrature method, as Gaussian support increases, with $M = 110$ (fixed), $\xi = 8$, $a = -0.1$, $b = 1.1$, $x' = 0.51$, $m = 8$.

In Figure 3 (left) we numerically demonstrate spectral convergence (24), $\|T_M(k) - \hat{f}(k)\|_\infty \sim \exp(-c(\beta)M^2)$ for some $c > 0$ that naturally depends on β .

We can go further with the 1D example and introduce the parameterization, $\beta = 2\xi^2/\eta$ in the transform pair (25), and *modus operandi* of the Gaussians in the fast method above. That is, let the domain $x \in (a, b)$ be discretized with M points, and let a Gaussian have support on P points around $x = x'$. Considering M fixed and increasing P , the discrete support of the truncated Gaussians, gives the convergence results in Figure 3 (right). Numerically, we have demonstrated that:

Remark 3.3. *The trivial 1D quadrature method (24) for the Fourier integral transform (25) (with $\beta = 2\xi^2/\eta$) converges, $\|T_{M,P,m}(k) - \hat{f}(k)\|_\infty \sim \exp(-c(m)P^2)$, independently of M and ξ .*

Hence, the quadrature required to get into frequency domain has the important characteristic that approximation errors are controlled by P , the resolution of Gaussians, alone (so that the grid size can be determined by a truncation estimate for the underlying Ewald sum). This numerical result is well supported by the analytical error analysis of our 3P fast Ewald method, cf. [37]. In essence – a Gaussian decays fast enough that no numerical difficulties arise from the oscillatory nature of the Fourier integral, so the trivial quadrature converges to machine precision with no need for e.g. *oversampling*.

3.2.2 Inverse Fourier integral transform of non-Gaussian via FFT

Having concluded that the mixed transform of the gridded charge distribution (17) into reciprocal space poses no particular numerical challenge, we turn to the relevant inverse

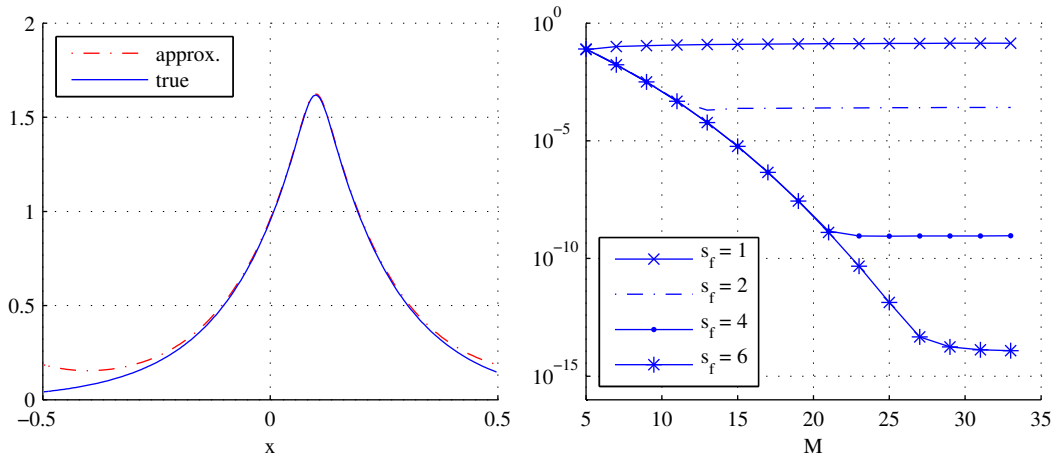


Figure 4: Inverse transform (26). Left: Illustration of non-converging errors when no oversampling ($s_f = 1$) is used. Right: Convergence of FFT-based quadrature from (25), up to a normalization, to the exact transform (26), $\xi = 8$.

transform. With (19) in mind we consider

$$\hat{f}(\kappa) = \frac{e^{-(1-\eta)(k_0^2 + \kappa^2)/(4\xi^2)}}{k_0^2 + \kappa^2} e^{i\kappa x'}, \quad k_0 = 2\pi/L,$$

and the inverse transform

$$f(x) = \frac{1}{2\pi} \int_{\mathbb{R}} \hat{f}(\kappa) e^{i\kappa x} d\kappa. \quad (26)$$

This integral does not offer an obvious closed form as in the previous example. None the less, for $\eta \leq 1$, the integrand is smooth and integrable on \mathbb{R} . In this particular section we employ arbitrary-precision integrators from *Mathematica 7*, so that the FFT-based quadrature method can be evaluated down to the regime of machine precision.

The quadrature method for the inverse transform is, up to a normalization, identical to the approximate forward transform (24). Again, we associate the reciprocal space grid $\frac{2\pi}{L} \{-M/2, \dots, M/2\} \ni k$ with a uniform staggered grid on the real-space interval $[a, b]$. However, we find that this reciprocal grid is too coarse. Instead we consider the family of *oversampled* grids, $\Delta\kappa \{-s_f M/2, \dots, s_f M/2\}$, $s_f \in \mathbb{Z}^+$, $\Delta\kappa = 2\pi/(s_f L)$. Evidently, with $s_f = 1$ there is no oversampling.

In Figure 4 we present numerical result for a sequence of grids. Note that without oversampling there are very visible artefacts of periodicity visible and no convergence. It is evident that this transform is significantly harder to compute than the transform of the pure Gaussian (cf. Section 3.2.1). That said – oversampling the FFTs by a small factor (up to six times for double precision accuracy) is well within the realm of practicality, as we shall return to. It is worth emphasizing that “oversampling” as we defined it here can be given various other equivalent meanings and monikers, such as “zero padding” and “ s points per wavelength”.

3.2.3 Extension to functions in V_Ω

The results from the 1D analyses generalize to the relevant 3D (or, rather, 2P) transforms directly. That is, the transform $H(\mathbf{r}, z) \rightarrow \hat{H}(\mathbf{k}, \kappa)$ is computed via a 3D FFT, where the

“third” FFT is thought of as a quadrature operation (and appropriate pre-factors enter). We let T^{2P} denote the immediate extension of the 1D quadrature scheme (24) on a grid $\bar{M} := [M_{xy}, M_{xy}, M_z]$. One may again pose this computation in terms of the “fixed-grid, variable Gaussian support”-setting. To no surprise, one immediately¹ finds that

$$\|T_{\bar{M}, P, m}^{2P}(\mathbf{k}, \kappa) - \hat{H}(\mathbf{k}, \kappa)\|_\infty \sim \exp(-c(m)P^2),$$

independently of \bar{M} and ξ . Again, this has theoretical justification in the error estimates of the 3P method [37]. The inverse transform $\hat{H}(\mathbf{k}, \kappa) \rightarrow \tilde{H}(\mathbf{r}, z)$, requires over-sampling by at least $s_f = 2$ in the third dimension, as in the 1D example.

The impatient reader may wonder why we have not precisely defined the quadrature methods in 2P including the pre-factors for both the forward and inverse transforms. The reason is that this somewhat laborious exercise in notation is not needed – between the forward and inverse transforms in the fast Ewald method, only a multiplication (19) occurs, so the pre-factors cancel by linearity. This suggests that we are back to “just 3D FFTs” as in pure 3P Ewald methods. Recall, though, that we are still in the 2P setting, computing (12) - (16) including the \mathbf{k} -singular contribution (15) which we discuss in Section 3.4. Additionally, we contend in the next section that an FFT-based quadrature method is efficient only when the underlying grid function is C^∞ smooth. In particular, adapting traditional PME-type methods to 2P, as in [28], leads to much greater numerical challenges.

3.2.4 Why not Cardinal B-splines and SPME?

The reader who is familiar with fast Ewald methods may wonder what role the charge-assignment scheme (17) plays for the computation of the mixed transform. We use Gaussians, $e^{-\alpha(x-x')^2}$, but that is by no means the only choice. The *Smooth Particle Mesh Ewald* (SPME) method [14], for instance, uses Cardinal B-splines in the corresponding step. These are given by

$$F_p(u) = \frac{1}{(p-1)!} \sum_{k=0}^p (-1)^k \frac{p!}{k!(p-k)!} (u-k)_+^{p-1}, \quad (x)_+ := \max(x, 0) = (x + |x|)/2, \quad (27)$$

where p is the order of the spline, and have a known Fourier transform:

$$\widehat{F}_p(k) = \frac{i(-1 + e^{ik})^p}{k^p}. \quad (28)$$

Indeed, Kawata and Mikami [28] propose a SPME-like method for the 2P case that uses this charge assignment function and their method is also based on the sum/integral (13). Thus, we ask how the the simple quadrature method (24) applied to (27) converges to (28). We note that $F_p \in C^p$ and $\widehat{F}_p \sim k^{-p}$. In Figure 5 we illustrate the expected convergence, M^{-p} , as the number of grid points in the quadrature method (24) grows. The contrast to the convergence in the Gaussian case, Figure 3, demands more than passing notice.

The loss of regularity by going from Gaussians to Cardinal B-splines is significant and it lies at the heart of our argument. An FFT-based quadrature method (as used here and in

¹Explicit numerical results for the Fourier integrals of 2P functions, analogous to Sections 3.2.1 and 3.2.2 are omitted for brevity and concern over repetition. The propositions of spectral accuracy of the quadrature in the mixed transforms (and the need to oversample the inverse transform) are supported by the numerical evaluation of the complete fast method, cf. Section 4.1.

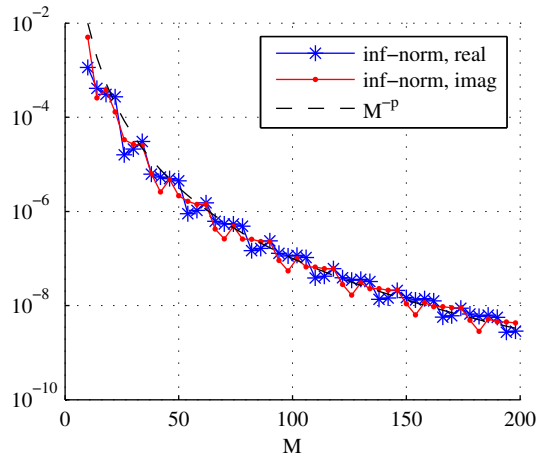


Figure 5: For Cardinal B-spline (27), convergence of FFT-based quadrature (24) to exact Fourier transform (28). As expected, the error behaves as M^{-p} (dashed line), where p is the order of the B-spline. Here, $p = 5$.

[28]) loses *a lot* of accuracy as Gaussians are replaced with B-splines in the integrand. The results given here indicate that hundreds of grid-points will be needed in the z -direction to compute the forward transform (analogous to the step $H(\mathbf{r}, z) \rightarrow \hat{H}(\mathbf{k}, \kappa)$) with decent accuracy. Additionally, we saw in Section 3.2.2 that the mixed inverse transform (in our case $\hat{H}(\mathbf{k}, \kappa) \rightarrow \tilde{H}(\mathbf{r}, z)$) is the main numerical challenge. We contend that it will be doubly so if Cardinal B-splines, or any other charge-assignment scheme from 3P PME methods, are used. The grid sizes and oversampling factors seen in [29, 28] seem to support this position.

3.3 Fast gridding

The expressions (17) and (21) involve computing N exponential functions for each point \mathbf{x} on the grid. If the grid has M^3 points this naively suggests NM^3 evaluations of $\exp(\cdot)$, which drops to NP^3 with the truncation from Section 3.1.1. This, as it turns out, is still many more than are needed if one uses the Gaussian gridding approach of Greengard and Lee [19].

The grid-representation of our source distribution (17), is a sum on the form

$$H(\mathbf{x}) = \left(\frac{\alpha}{\pi}\right)^{3/2} \sum_{n=1}^N q_n e^{-\alpha \|\mathbf{x} - \mathbf{x}_n\|^2}. \quad (29)$$

For clarity here we shall suppose that the Gaussians are not truncated. The key observation is that we wish to evaluate $H(\mathbf{x})$ on an equidistant grid, i.e. $\mathbf{x} = [ih, jh, kh]$, where (i, j, k) are integer index triplets in the range $0, 1, \dots, M - 1$. To see how we can reduce the number of computations of $\exp(\cdot)$, take the analogous 1D Gaussian,

$$\begin{aligned} e^{-\alpha(x-x_n)^2} &= e^{-\alpha(ih-x_n)^2} = e^{-\alpha((ih)^2 - 2ihx_n + x_n^2)} \\ &= \underbrace{e^{-\alpha(ih)^2}}_{(a)} \underbrace{\left(e^{2\alpha h x_n}\right)^i}_{(b)} \underbrace{e^{-\alpha x_n^2}}_{(c)}. \end{aligned} \quad (30)$$

Note that the term (a) is independent of x_n , so those M evaluations of $\exp(\cdot)$ are done once, stored and reused for each of the N sources x_n . The terms (b) and (c) each incur one $\exp(\cdot)$

for each x_n . The same procedure is then applied for $e^{-\alpha(y-y_n)^2}$ and ditto for z . For full algorithms, additional details and *important* remarks, we refer to [37]. The bottom line is that, rather than having to compute NP^3 exponentials, the gridding step requires $P^3 + 4N$ exponentials and $\mathcal{O}(NP^3)$ multiplications. This translates to a significant performance gain in practice.

3.4 Fast method for $\varphi^{F,\mathbf{k}=0}$

Turning now to an efficient and accurate method for evaluating the singular part of the reciprocal space 2P Ewald sum: The computation of (15),

$$\varphi_m^{F,\mathbf{k}=0} = \varphi^{F,\mathbf{k}=0}(z_m) = -\frac{2\sqrt{\pi}}{L^2} \sum_{n=1}^N q_n f(z_m - z_n) \quad (31)$$

$$f(z) = e^{-\xi^2 z^2} / \xi + \sqrt{\pi} z \operatorname{erf}(\xi z), \quad (32)$$

is much less complex than the fast computation of (13) – it is a finite sum over terms that only depend on z . The obvious approach to avoid $\mathcal{O}(N^2)$ complexity is an appropriate interpolation method (sometimes imprecisely referred to as *table lookup*), and the natural choice is to use Chebyshev polynomials. This method is close to optimal in ∞ -norm and cheap to compute (even though there is no periodicity in $\varphi^{F,\mathbf{k}=0}(z)$). More precisely, we have $z_n \in [0, L_z]$, and let $p_k, k = 1, 2, \dots, M_T \ll N$, be the set *Chebyshev-Gauss* points $\cos(\pi(2k-1)/(2M_T))$ scaled to the interval $[0, L_z]$. We expand $\varphi^{F,\mathbf{k}=0}$ in terms of Chebyshev polynomials

$$\varphi^{F,\mathbf{k}=0}(z) \approx T(z) = \sum_{j=1}^{M_T} c_j T_j^{[0,L_z]}(z), \quad \varphi^{F,\mathbf{k}=0}(p_k) = T(p_k),$$

where $T_j^{[0,L_z]}(z)$ is the j :th Chebyshev polynomial scaled to the relevant interval. The coefficients c_j are easily computed after evaluating $\varphi^{F,\mathbf{k}=0}(p_k)$, and M_T is in essence an accuracy parameter – so the complexity of this task is $\mathcal{O}(N)$. We are dealing with interpolation in 1D, so the computational resources involved are entirely trivial². Note that the well-known Clenshaw formula should, for reasons of numerical stability, be used when evaluating the orthogonal basis $\sum c_j T_j(z)$.

Very strong error bounds exist for Chebyshev interpolation (see e.g. the classical references Rivlin [47, 48]), such as

$$e_M := \max_{z \in [0, L_z]} |f(z) - T^f(z)| \leq \frac{f^{(M_T)}(c)}{2^{M_T-1} M_T!},$$

for some $c \in [0, L_z]$, where T^f is the interpolant of order M_T to f (32). It is evident that f possesses M_T derivatives. However, each differentiation yields roughly a factor ξ^2 , so the interpolation error will ultimately depend on ξ . This suggests an interpolation estimate of the form $e_M \approx C \xi^{M_T} 2^{-(M_T-1)} / M_T!$, but that turns out to be impractical and inaccurate due to the very large quantities involved. Instead, we find that

$$e_M \approx \xi^3 2^{-c(M_T-1)}, \quad c = \pi \xi^{-1/2}, \quad (33)$$

²As a point of reference, with $N = 10^6$ particles and $M_T = 40$ Chebyshev polynomials it takes roughly one second to evaluate $\varphi^{F,\mathbf{k}=0}(z_m)$ at all points $z_m, m = 1, \dots, 10^6$.

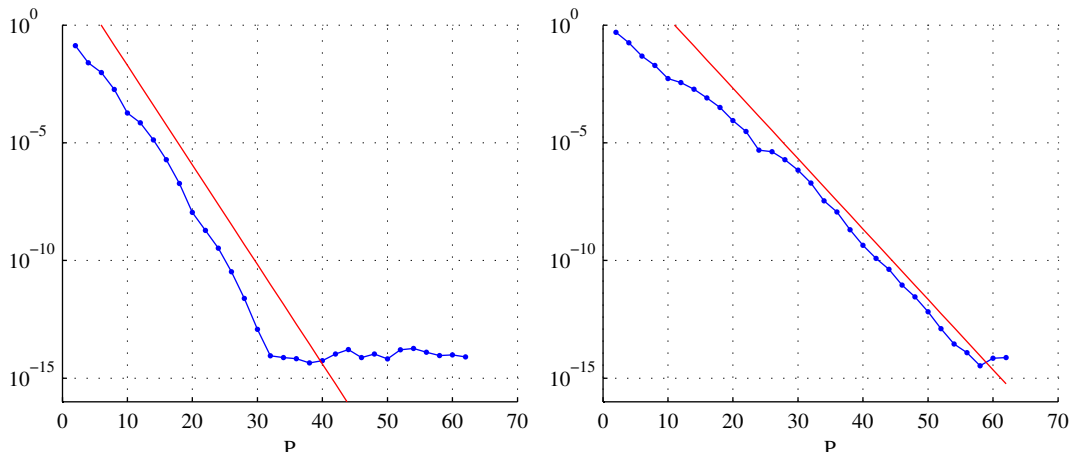


Figure 6: Error in ∞ -norm when computing $\varphi^{F, \mathbf{k}=0}$ with Chebyshev interpolation, with $N = 10$, together with “practical” error estimate (33). Left: $\xi = 5$. Right: $\xi = 10$.

provides a useful form. Again, one may treat error estimation here with some laxity, as the performance penalties associated with being cautious (i.e. taking M_T needlessly large) are *very* small. We give brief numerical results in Figure 6.

In their method, Kawata and Mikami [28] propose a similar approach based on B-splines. These, of course, have polynomial accuracy order. A small numerical experiment (omitted) indicates that the previous remarks about computational triviality then fail to apply (at least in the broad accuracy regime considered).

3.5 Error analysis

We now gather strands of numerical and theoretical results into an aggregate view of the numerical properties of the proposed method. This serves the dual purposes of putting previous statements of accuracy on secure theoretical foundations, and providing useful guidance for the often intricate task of parameter selection. As previously alluded to, we start from the classification of numerical errors into two categories: errors that stem from the underlying Ewald sum (4) and errors that stem from the fast method of the present section.

3.5.1 Truncation estimates for Ewald sums

Turning to the 2P Ewald sums for φ^R (12) and φ^F (14), we note that both sums are infinite but rapidly converging. The real space sum (12) is unchanged *vis-a-vis* 3P, and has been thoroughly studied in that context. The reader may already be familiar with the famous error estimates by Kolafa and Perram [34], which suggest that the truncation error committed by letting $\|\mathbf{x}\| < r_c$ may be estimated by

$$e_{\text{rms}}^R(r_c, \xi) \approx \sqrt{\frac{Q}{2L^3}} (\xi r_c)^{-2} e^{-r_c^2 \xi^2}, \quad (34)$$

where $Q := \sum_{n=1}^N q_n^2$ and the RMS norm is defined as $e_{\text{rms}} := \sqrt{N^{-1} \sum_{n=1}^N (\varphi_n - \varphi^*(\mathbf{x}_n))^2}$. If particles are statistically correlated, i.e. not randomly scattered, an ∞ -norm measure may be more appropriate, see e.g. Strain [51].

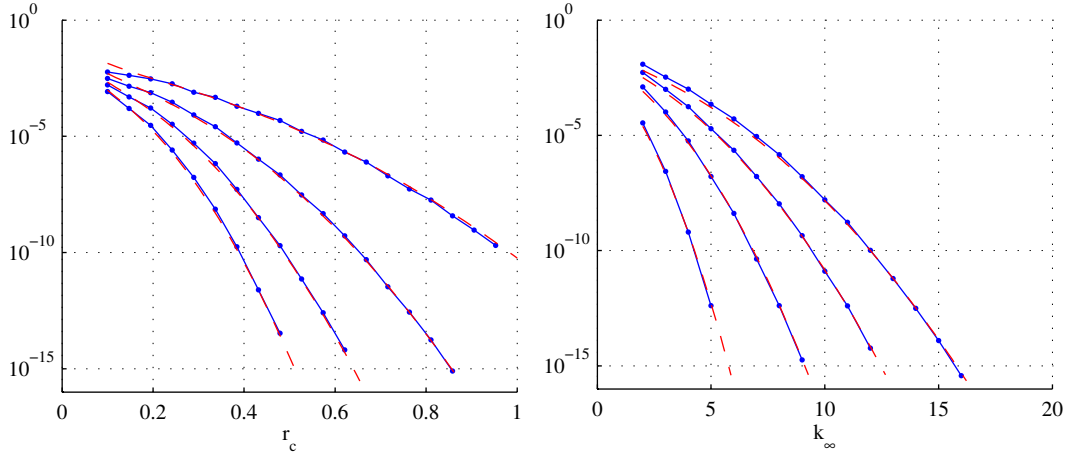


Figure 7: Left: Convergence of real-space sum (12) as function of truncation radius, $\|\mathbf{x}\| < r_c$, for (right to left) $\xi = 4, 6, 8, 10$ and the error estimate (34) in dashed. Right: convergence of \mathbf{k} -space sum (14) as a function of the truncation, $\|\mathbf{k}\| \leq 2\pi k_\infty/L$, for (left to right) $\xi = 4, 6, 8, 10$ and the error estimate (35) in dashed.

Correspondingly, for the 3P \mathbf{k} -space Ewald sum – truncated at finite number of modes, $k_\infty \in \mathbb{Z}^+$, i.e. $\|\mathbf{k}\| \leq 2\pi k_\infty/L$ – Kolafa & Perram [34] suggest that

$$e_{\text{rms}}^F(k_\infty, \xi) \approx \xi \pi^{-2} k_\infty^{-3/2} \sqrt{Q} \exp\left(-\left(\frac{\pi k_\infty}{\xi L}\right)^2\right). \quad (35)$$

The feasibility of (35) as a 2P estimate may come as a surprise, as it arose from analysis of the 3P sum. We contend that this is quite natural – roughly speaking, each dimension has to converge. Figure 7 shows numerically that (34) and (35) capture the behavior of the truncation error with striking agreement.

3.5.2 Approximation errors

The second family of errors are those that stem from the fast method, described in the preceding sections, notably the error due to the quadrature used to evaluate (21). An extensive treatment is given in [37], where we prove the following theorem:

Theorem 3.4 (Error estimate). *Given $\xi > 0$, $h > 0$ and an odd integer $P > 0$, let $w = hP/2$, and define η according to (22). The error incurred in evaluating (21) by truncating the Gaussian at $\|\mathbf{x} - \mathbf{x}_m\| = w$ and applying the trapezoidal rule T_P can be estimated by*

$$|\varphi - T_P| \leq C \left(e^{-\pi^2 P^2 / (2m^2)} + \text{erfc}\left(m/\sqrt{2}\right) \right). \quad (36)$$

From this we surmise an appealing choice of the shape parameter, $m(P) \approx \sqrt{\pi P}$, which then yields a quadrature error estimate

$$E_Q(P) := |\varphi^F - T_P| \approx C e^{-\pi P/2}, \quad (37)$$

to be verified in Section 4.1. Two other errors emerge, specific to the 2P method: First, there is an interpolation error from the fast method for $\varphi^{F, \mathbf{k}=0}$, as we investigated in Section

3.4. Secondly, there is the need to oversample the inverse transform when computing $\tilde{H}(\mathbf{r}, z)$, which we devoted Section 3.2.2 to. We view the oversampling guidelines from Figure 4 as generally applicable, and content ourselves with that.

3.5.3 Choosing parameters

There are several parameters present in all (fast) Ewald methods and they should be chosen with two goals in mind: balancing the work between the real- and \mathbf{k} -space sums (by choosing ξ), and attaining a desired accuracy (selecting e.g. an appropriate PME grid M). The first concern is inherently implementation-dependent and work-balance will depend strongly on N , the number of charges. *Ipsa facto*, there can not exist an optimal parameter set of broad applicability, and there is no generally accepted tuning method.

The second concern, assuring that the end-result satisfies a desired accuracy is also an open question (and likely to remain that way). Two approaches stand out in the literature: using an optimization technique, and relying on *a priori* error estimates. Among the advocates of “optimization”³ are Kawata et. al. [32] and Ghasemi et. al. [18]. The former (cf. [32, Tab. 2], where eight parameters are determined) suggest a high degree of irregularity in the parameter set (which is either incorrect *per se* or grounds for concern over the numerics involved). In the latter work, “Pareto frontier optimization” is used (on a set of five parameters) for a specific crystalline system. In both cases, it is implied that a similar investigation should be performed whenever a new system is under consideration – but the optimization technique depends on a sufficiently accurate reference solution being computable by the underlying Ewald sum, which naturally restricts the method to small N .

On the other hand, relying on *a priori* error analysis alone has to confront a complicated mix of numerical errors. Whereas the picture is clear for pure 3P Ewald summation (2), as we discuss in Section 3.5.1, fast methods often pose stiff challenges to error estimation. In their survey of fast 3P methods, Deserno and Holm [11] sketch the parameter space and remind us that many numerical errors are interdependent. Methods for the 2P situation are less mature and fewer error estimates have been established. A notable exception is the MMM2D method by Holm et. al. [3, 2], which enjoys sharp error estimates that are suitable for parameter selection. In [8], they provide analysis for the case when the 3P Ewald sum is used for 2P systems, though results are absent for the PME-accelerated case.

Our view is that error analysis should be the primary focus, but a certain amount of experimentation is a worthy complement. A particular goal is to have errors that decouple, so that parameters can be chosen in sequence and numerical experiments can treat one parameter at a time. This is by no means simple – established PME methods for the 3P Ewald sum have approximation and truncation errors in a tangle after doing charge-assignment by e.g. B-splines, as we elaborate on in [37] – but in the present work decoupling is achieved. Furthermore, to be useful, error estimates need to be sharp and simple enough that they are “solvable” for a desired parameter.

As a sequence of considerations we suggest

1. Determine a truncation radius, r_c , such that the real space sum is cheap to compute (cf. *neighbor list* methods [1] or as summarized in [37]).

³A more correct description of the parameter optimization problem may be “scanning”, and should generally not be confused with numerical optimization techniques (such as gradient-based methods).

2. Select Ewald parameter, ξ , such that the real space sum has converged to within a given tolerance, ε , at $\|\mathbf{r}\| < r_c$ by invoking e.g. (34),

$$\xi = \frac{1}{r_c} \sqrt{W \left(\frac{1}{\varepsilon} \sqrt{\frac{Q}{2L^3}} \right)}, \quad (38)$$

where $W(\cdot)$ is the *Lambert W-function* (also known as the *product logarithm*, it is among the “special functions” provided in e.g. Matlab and Mathematica, defined as the inverse of $f(W) = We^W$ [5]).

3. Then determine the truncation, k_∞ , of the \mathbf{k} -space Ewald sum (4), such that the same tolerance is met, from (35):

$$k_\infty > \frac{\sqrt{3}L\xi}{2\pi} \sqrt{W \left(\frac{4Q^{2/3}}{3\pi^{2/3}L^2\xi^{2/3}\varepsilon^{4/3}} \right)}. \quad (39)$$

This gives the grid size to be employed in the spectral PME method: $M = 2k_\infty$.

4. The quadrature error estimate (37), implies the number of points within the support of each Gaussian:

$$P > -\frac{2L \log(\varepsilon/C)}{\pi}.$$

Note that one may get $P > M$ (if ξ small), in which case one has to increase the grid size, i.e. $M = \max(P, 2k_\infty)$. The constant, C , here (from the error estimate (37)) does not depend on ξ , so P is perhaps most conveniently identified from a basic convergence test, e.g. Figure 8 where the estimate is plotted with $C = 10$.

5. Select a oversampling factor, s_f , for the reciprocal space calculations of the fast method, as discussed in Section 3.2.
6. Finally, determine the Chebyshev grid (cf. Section 3.4) for computing $\varphi_m^{\mathbf{k}=0}$ (15).

If this sequence of steps seems laborious, it might be worth pointing out that having a spectrally accurate method at hand makes it cheap to err on the side of caution – the parameter with the greatest impact on run-time is P . Again, it’s a sequential process – rather than a non-linear optimization problem.

4 Numerical Evaluation

4.1 Accuracy of spectral PME method

In Section 3.5 we showed that convergence of the order $e^{-\alpha P}$ is to be expected (we have taken $m = 0.91\sqrt{\pi P}$). To test this we consider small systems, so that the 2P Ewald sum (4) can be accurately computed as a reference, denoted φ^* , and measure errors in the following norm:

$$e := \frac{1}{N} \sum_{m=1}^N |\varphi^F(\mathbf{x}_m) - \varphi^*(\mathbf{x}_m)|. \quad (40)$$

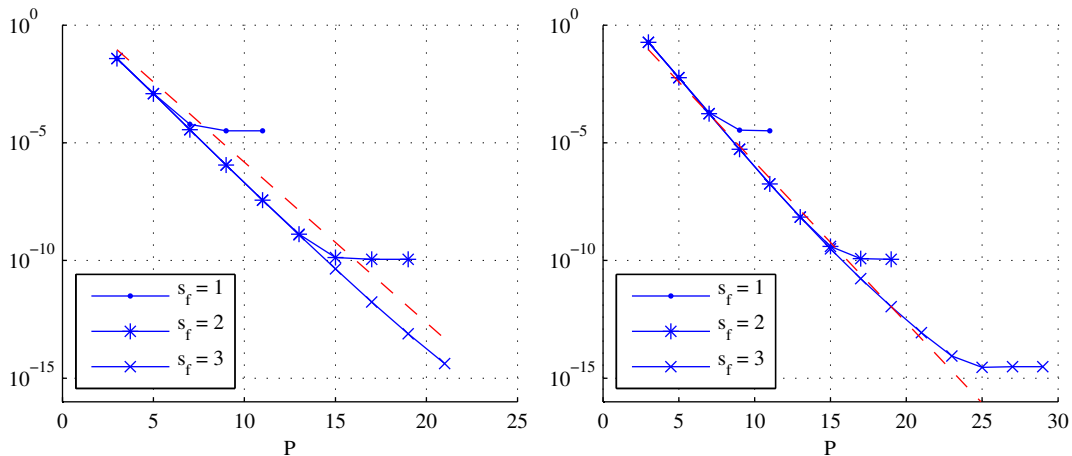


Figure 8: Convergence of SE2P method to Ewald sum, in norm (40), for various oversampling factors, with quadrature error estimate (37) as dashed line. The computational domain is $[0, 1)^2 \times [-1/2, 3/2]$, so $M_z = 2s_f M$. Left: $\xi = 4$, $M = 21$. Right: $\xi = 12$, $M = 50$.

We draw $\mathbf{x}_m \in [0, 1)^3$ from a uniform random distribution, randomize charges under the constraints that $\sum q_m = 0$ and $\sum |q_m| = 1$. The minimal computational domain is $[0, 1)^2 \times [-w, 1 + w]$, but as $w = w(P)$ we take $[0, 1)^2 \times [-1/2, 3/2]$ to avoid having a PME-grid that depends on P . We take $N = 50$, consider two cases: $\xi = 4$, $M = 21$ and $\xi = 12$, $M = 50$. The convergence results in Figure 8 support several conclusions: (i) spectral accuracy as predicted by theory; (ii) convergence rate independent on Ewald parameter ξ ; (iii) oversampling the grid in the z -direction by a factor three (or six as $L_z = 2L_{x,y}$, i.e. $M_z = 2s_f M = 6M$, depending on how you look at it) is sufficient to get double precision accuracy.

4.2 Computational overview

To give a sense of the practical characteristics of our method, we give a brief overview of the run-time profile with our implementation. We have previously discussed the need to oversample the Fourier transform in the z -direction, and the question then naturally arises if this incurs a significant cost. We note that the (x, y) -grid is $M \times M$ and, by the error analysis presented, M rarely needs to be bigger than 50. Hence, even in the case where we oversample by a factor 6 – to safely commit an quadrature error in the Fourier integral transform on the order of machine accuracy, cf Section 3.2 – the total grid size is $6 \times 50^3 = 750000$ elements (stored in about 6MB). In the works cited, grid sizes of up to 512^3 are mentioned (at much more modest accuracies).

As expected then, the computational burden in our method falls on the gridding steps (17) and (21). We illustrate this for two systems in Figure 9. Here we let $\xi = 8$ and target an accuracy $\varepsilon \approx 10^{-10}$ (see caption for further details). These are single-core results obtained on an ordinary workstation computer (Intel Core2Duo E6600), implementation in C. In Table 1 we give performance numbers for the gridding step in terms of the support P .

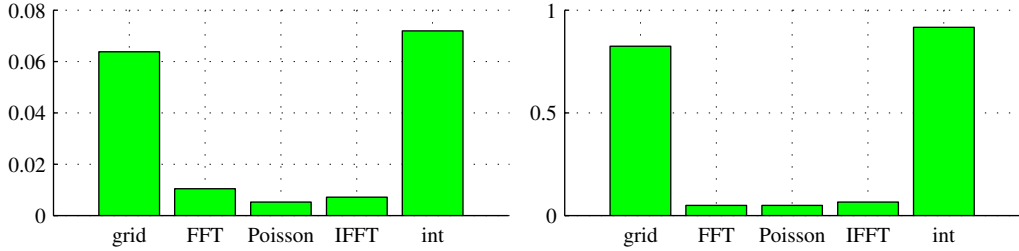


Figure 9: Runtime profile, i.e. time spent in different parts of fast algorithm, where “grid” refers to (17), “Poisson” refers to (19) and “int” refers to (21). Left: $N = 10000, M = 20, P = 15$. Right: $N = 10^5, M = 40, P = 17$. In both cases FFT oversampled by factor six in z -direction, $M_z = 6M$. Despite that, the transforms take a trivial amount of time to compute.

$P =$	3	7	11	15	19	23
time [μs]	0.73	1.67	3.36	7.48	13.57	23.49

Table 1: Time for gridding (in microseconds per particle) for different support P .

4.3 Scaling to large systems

Computing the real-space sum (12) has been ignored up to this point, save for the remarks on parameter selection of Section 3.5.3. In this regard we follow the conventional line of thought – computing (12) has $\mathcal{O}(N)$ complexity *iff* each particle interacts with a *fixed* number of neighbors that lie within a radius r_c , as N grows. This implies either (i) that the domain grows (so that N/L^3 constant, and r_c constant), or (ii) that the interaction radius, r_c , decreases, as N grows. Regardless, the grid size, M , will grow.

Following the second approach, we return to the parameter estimates in Section 3.5.3 and note, by (38), that ξ grows as r_c becomes smaller. Consequently, and by (39), the grid size M will grow with N . Hence, the complexity of our proposed spectrally accurate PME method is $\mathcal{O}(N \log N)$. Note that before the $\mathcal{O}(N)$ complexity of the real space sum is imposed, the calculations (17) - (21) have complexity $\mathcal{O}(NP^3) + \mathcal{O}(M^3 \log M^3) = \mathcal{O}(N)$. As we suggest in the previous section, the constant in front of the first term is quite a bit bigger than the constant in the FFT part. Thus, the $\log N$ factor is not seen in practice.

To verify this, and clarify the parameter selection process (cf. Section 3.5.3), we give scaling results (measured run-time to compute φ^F) in Figure 10, including the parameter table (right). Here, the target accuracy is $\varepsilon = 10^{-9}$, we start with $N = 1000$ and let $P = 15$, and invoke the estimates as described.

5 Summary and concluding remarks

In our survey of methods to compute the sum of Coulomb potentials (1) we argue that methods for the 2P case are less mature and consistent than their 3P cousins. Hence, the desire from the applications community for an established tool for 2P electrostatic calculations is to some extent unsatisfied.

We aim to close the gap between 2P and 3P Ewald methods by two provisions. First, we derive the 2P Ewald sum (4) using the established methodology of screening functions that

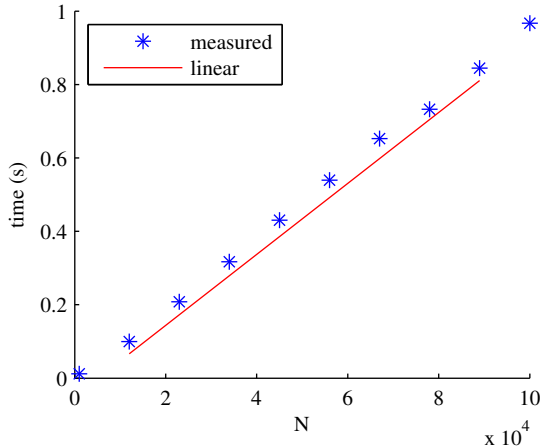


Figure 10: Left: Run-time as a function of N , with $\varepsilon = 10^{-9}$. Right: Parameters to scale up system at constant cost for real-space sum

follows the 3P case closely (Section 2.2). Secondly, we derive a fast PME-type method for the 2P \mathbf{k} -space sum that fits well in the established PME framework (Section 3.1), which we refer to as SE2P. These derivations were made possible by representing functions on mixed periodicity (x, y periodic, z “free”) in frequency domain via a mixed Fourier transform (5), see Section 2.1. This point of view is natural and clarifies the relationship between 2P and 3P Ewald methods to an extent that we do not believe has been previously reported.

In light of this, we conclude that a fast PME-type method for 2P will have to compute a mixed transform (a discrete Fourier transform in the periodic variables, and an approximation to the continuous Fourier integral transform in the free dimension). Efficiency constraints suggest that the quadrature for the Fourier integral should be based on the FFT. We studied this problem in Section 3.2, and point out that the accuracy of an FFT-based quadrature method will depend on the regularity of the integrand.

Hence, a method using the SPME approach (using Cardinal B-splines to represent regularized charges on the grid) will have to deal with vastly reduced accuracy in the quadrature step of the Fourier transform *vis-a-vis* the approach that we suggest, which uses Gaussians that are C^∞ smooth. Whereas established PME methods may be seen as adequate, in terms of accuracy, for the 3P case, our analysis suggest that that may not be true in 2P (Section 3.2.4). The SE2P method is similar in structure to the work by Kawata et. al. [28], though it appears to offer significant advantages.

The method we propose (Sections 3.1 to 3.3) for computing the 2P \mathbf{k} -space Ewald sum is spectrally accurate, meaning that all errors decay exponentially (as we establish theoretically in Section 3.5 and verify numerically in Section 4.1). More specifically, the numerical errors present stem from two sources: truncation of the underlying Ewald sum (Section 3.5.1) and approximation errors introduced by the fast method (Section 3.5.2). A well established error estimate for the former is used to determine the appropriate grid size, M . Our error analysis of the latter is used to determine the number of points within the support of our Gaussians, P . To our knowledge, this is the only fast Ewald summation method that is spectrally accurate and the only one that retains a decoupling of errors as discussed here – *a fortiori* in 2P.

Moreover, the proposed method is efficient, capable of dealing with $N \sim 10^6$ in a few seconds (Section 4.2). In particular, we see that the grid sizes needed are very small – so

small that the Fourier transforms are cheap to compute, even when allowing for oversampling the z -dimension. The computational burden falls more heavily on the gridding steps (17) and (21). The Fast Gaussian Gridding approach (Section (3.3)) alleviates this to a large extent.

We believe that these properties – accuracy, clear parameter selection, efficiency, and closeness to 3P methods – present a compelling case for the proposed method for electrostatic calculations in planar periodicity.

Acknowledgments

A.K.T. is a Royal Swedish Academy of Sciences Research Fellow supported by a grant from the Knut and Alice Wallenberg Foundation and thankfully acknowledges this support.

A Derivation of 2P Ewald sum, details

The derivation of $\varphi^{F,\mathbf{k}=0}(z)$, the singularity contribution (15), is given here for completeness and because it's illuminating in it's own right.

To make this clear, we first disregard the screening, γ , i.e. consider

$$-\Delta\varphi(\mathbf{x}) = 4\pi \sum_{n=1}^N \rho^n(\mathbf{x}), \quad \rho^n(\mathbf{x}) = \sum_{\mathbf{p} \in \mathbb{Z}^2} q_n \delta(\mathbf{x} - \mathbf{x}_n + \tilde{\mathbf{p}}),$$

under an assumption of charge neutrality, $\sum_{n=1}^N q_n \equiv 0$, and the condition

$$\lim_{z \rightarrow \pm\infty} \varphi(\mathbf{x}) = \pm \frac{2\pi}{L^2} \sum_{n=1}^N q_n z_n. \quad (41)$$

Provisionally, as in Section 2.2,

$$\varphi(\mathbf{r}, z) \sim \frac{2}{L^2} \sum_{\mathbf{k}} \int_{\mathbb{R}} \frac{1}{k^2 + \kappa^2} \sum_{n=1}^N q_n e^{i\mathbf{k} \cdot (\mathbf{r} - \mathbf{r}_n)} e^{i\kappa(z - z_n)} d\kappa.$$

The terms corresponding to $\mathbf{k} \neq 0$ are uncomplicated and can be integrated,

$$\begin{aligned} \tilde{\varphi}(\mathbf{r}, z) &:= \frac{2}{L^2} \sum_{\mathbf{k} \neq 0} \int_{\mathbb{R}} \frac{1}{k^2 + \kappa^2} \sum_{n=1}^N q_n e^{i\mathbf{k} \cdot (\mathbf{r} - \mathbf{r}_n)} e^{i\kappa(z - z_n)} d\kappa \\ &= \frac{2\pi}{L^2} \sum_{\mathbf{k} \neq 0} \sum_{n=1}^N q_n \frac{1}{\|\mathbf{k}\|} e^{-\|\mathbf{k}\||z - z_n|} e^{i\mathbf{k} \cdot (\mathbf{r} - \mathbf{r}_n)}. \end{aligned} \quad (42)$$

Note that $\lim_{z \rightarrow \pm\infty} \tilde{\varphi} = 0$. Hence, we seek a term $\varphi^0(z)$ with the desired behavior (41) at $z \rightarrow \pm\infty$. Then, $\varphi(\mathbf{x}) = \tilde{\varphi}(\mathbf{x}) + \varphi^0(z)$ will be a unique and well defined solution to the 2-periodic Poisson problem under consideration.

If we disregard the boundary condition (41), it's evident that φ is only determined up to a piecewise linear function. Consider the adding the term $\varphi^0(z) = b \sum_{n=1}^N q_n |z - z_n|$. Using charge neutrality, one finds that

$$\lim_{x \rightarrow \pm\infty} \varphi^0(z) = \mp b \sum_{n=1}^N q_n z_n.$$

This solution, with $b = -\frac{2\pi}{L^2}$, can be found e.g. by considering the one-dimensional Green's function for the $\mathbf{k} = 0$ mode, see Genovese et. al. [17]. With this,

$$\varphi(\mathbf{r}, z) = \frac{2\pi}{L^2} \sum_{\mathbf{k} \neq 0} \sum_{n=1}^N q_n \frac{1}{\|\mathbf{k}\|} e^{-\|\mathbf{k}\||z-z_n|} e^{i\mathbf{k} \cdot (\mathbf{r}-\mathbf{r}_n)} - \frac{2\pi}{L^2} \sum_{n=1}^N q_n |z - z_n|$$

satisfies (41).

There's a natural correspondence between $\tilde{\varphi}$ and φ^F (14). However, the crucial point when the decomposition (6) enters is that some of the $\mathbf{k} = 0$ mode will be included into the real-space sum. Therefore, rather than taking $\varphi^{F, \mathbf{k}=0}$ equal to φ^0 , we subtract the real-space term (which is most accessible as the difference between $\tilde{\varphi}$ and φ^F),

$$\varphi^{F, \mathbf{k}=0}(z) = \varphi^0(z) - \lim_{\mathbf{k} \rightarrow 0} \left(\widehat{\tilde{\varphi}}_{\mathbf{k}} - \widehat{\varphi^F}_{\mathbf{k}} \right).$$

We introduce

$$\lim_{\mathbf{k} \rightarrow 0} \left(\widehat{\varphi^F}_{\mathbf{k}} - \widehat{\tilde{\varphi}}_{\mathbf{k}} \right) = \frac{\pi}{L^2} \sum_{n=1}^N q_n a(z - z_n),$$

and compute

$$\begin{aligned} a(z) &= \lim_{k \rightarrow 0} \frac{1}{k} \left(e^{kz} \operatorname{erfc} \left(\frac{k}{2\xi} + \xi z \right) + e^{-kz} \operatorname{erfc} \left(\frac{k}{2\xi} - \xi z \right) - 2e^{-k|z|} \right) \\ &= -\frac{2}{\sqrt{\pi}} \left(\frac{1}{\xi} e^{-\xi^2 z^2} + \sqrt{\pi} (-|z| + z \operatorname{erf}(\xi z)) \right). \end{aligned}$$

Finally,

$$\begin{aligned} \varphi^{F, \mathbf{k}=0}(z) &= \frac{\pi}{L^2} \sum_{n=1}^N q_n a(z - z_n) - \frac{2\pi}{L^2} \sum_{n=1}^N q_n |z - z_n| \\ &= -\frac{2\sqrt{\pi}}{L^2} \sum_{n=1}^N q_n \left(\frac{1}{\xi} e^{-\xi^2 (z-z_n)^2} + \sqrt{\pi} (z - z_n) \operatorname{erf}(\xi(z - z_n)) \right), \end{aligned}$$

as we set out to show. Using charge neutrality, the limits (41) can be verified.

References

- [1] M. P. Allen and D. J. Tildesley. *Computer Simulation of Liquids*. Oxford University Press, 1989.
- [2] A. Arnold, J. de Joannis, and C. Holm. Electrostatics in periodic slab geometries. I. *J. Chem. Phys.*, 117:2496–2502, 2002.
- [3] A. Arnold and C. Holm. A novel method for calculating electrostatic interactions in 2D periodic slab geometries. *Chem. Phys. Lett.*, 354:324–330, 2002.
- [4] F. Bertaut. L'énergie électrostatique de réseaux ioniques. *J. Phys. Radium*, 13:499, 1952.

- [5] R. M. Corless, G. H. Gonnet, D. E. G. Hare, D. J. Jeffrey, and D. E. Knuth. On the Lambert W function. *Adv. Comput. Math.*, 5:329–359, 1996.
- [6] P. S. Crozier, R. L. Rowley, E. Spohr, and D. Henderson. Comparison of charged sheets and corrected 3D Ewald calculations of long-range forces in slab geometry electrolyte systems with solvent molecules. *J. Chem. Phys.*, 112:9253–9257, 2000.
- [7] T. Darden, D. York, and L. Pedersen. Particle Mesh Ewald - an N.log(N) method for Ewald sums in large systems. *J. Chem. Phys.*, 98:10089–10092, 1993.
- [8] J. de Joannis, A. Arnold, and C. Holm. Electrostatics in periodic slab geometries. II. *J. Chem. Phys.*, 117:2503–2512, 2002.
- [9] S. W. de Leeuw and J. W. Perram. Electrostatic lattice sums for semi-infinite lattices. *Mol. Phys.*, 37:1313–1322, 1979.
- [10] S. W. de Leeuw, J. W. Perram, and E. R. Smith. Simulation of electrostatic systems in periodic boundary conditions. i. lattice sums and dielectric constants. *Proc. Royal Soc. London A*, 373:27–56, 1980.
- [11] M. Deserno and C. Holm. How to mesh up Ewald sums. I. A theoretical and numerical comparison of various particle mesh routines. *J. Chem. Phys.*, 109:7678–7693, 1998.
- [12] A. Dutt and V. Rokhlin. Fast Fourier-transforms for nonequispaced data. *SIAM J. Sci. Comput.*, 14:1368–1393, 1993.
- [13] A. Erdélyi, editor. *Tables of Integral Transforms, Vol. 1*. McGraw-Hill, 12 1954.
- [14] U. Essmann, L. Perera, M. L. Berkowitz, T. Darden, H. Lee, and L. G. Pedersen. A smooth particle mesh Ewald method. *J. Chem. Phys.*, 103:8577–8593, 1995.
- [15] P. Ewald. Die berechnung optischer und elektrostatischer gitterpotentiale. *Ann. Phys.*, 64:253–287, 1921.
- [16] L. N. G Filon. On a quadrature formula for trigonometric integrals. *Proc. R. Soc. Edinburgh*, 49:38–47, 1928.
- [17] L. Genovese, T. Deutsch, and S. Goedecker. Efficient and accurate three-dimensional Poisson solver for surface problems. *J. Chem. Phys.*, 127, 2007.
- [18] S. A. Ghasemi, A. Neelov, and S. Goedecker. A particle-particle, particle-density algorithm for the calculation of electrostatic interactions of particles with slablike geometry. *J. Chem. Phys.*, 127, 2007.
- [19] L. Greengard and J. Y. Lee. Accelerating the nonuniform fast Fourier transform. *SIAM Rev.*, 46:443–454, 2004.
- [20] A. Grzybowski, E. Gwozdz, and A. Brodka. Ewald summation of electrostatic interactions in molecular dynamics of a three-dimensional system with periodicity in two directions. *Phys. Rev. B*, 61:6706–6712, 2000.
- [21] D. M. Heyes. Electrostatic potentials and fields in infinite point-charge lattices. *J. Chem. Phys.*, 74:1924–1929, 1981.

- [22] D. M. Heyes. Molecular-dynamics of ionic solid and liquid surfaces. *Phys. Rev. B*, 30:2182–2201, 1984.
- [23] D. M. Heyes, M. Barber, and J. H. R. Clarke. Molecular-dynamics computer-simulation of surface properties of crystalline potassium-chloride. *J. Chem. Soc Farad. T. 2*, 73:1485–1496, 1977.
- [24] D. M. Heyes and F. van Swol. The electrostatic potential and field in the surface region of lamina and semi-infinite point-charge lattices. *J. Chem. Phys.*, 75:5051–5058, 1981.
- [25] R. W. Hockney and J. W. Eastwood. *Computer Simulation Using Particles*. IOP, 1998.
- [26] A. Iserles. On the numerical quadrature of highly-oscillating integrals I: Fourier transforms. *IMA J. Numer. Anal.*, 24:365–391, 2004.
- [27] A. Iserles and S. Nørsett. On quadrature methods for highly oscillatory integrals and their implementation. *BIT*, 44:755–772, 2004.
- [28] M. Kawata and M. Mikami. Rapid calculation of two-dimensional Ewald summation. *Chem. Phys. Lett.*, 340:157–164, 2001.
- [29] M. Kawata, M. Mikami, and U. Nagashima. Rapid calculation of the Coulomb component of the stress tensor for three-dimensional systems with two-dimensional periodicity. *J. Chem. Phys.*, 115:4457–4462, 2001.
- [30] M. Kawata, M. Mikami, and U. Nagashima. Computationally efficient method to calculate the Coulomb interactions in three-dimensional systems with two-dimensional periodicity. *J. Chem. Phys.*, 116:3430–3448, 2002.
- [31] M. Kawata, M. Mikami, and U. Nagashima. Response to “Comment on ‘Rapid calculation of the Coulomb component of the stress tensor for three-dimensional systems with two-dimensional periodicity’ “ [J. Chem. Phys. 117, 3524 (2002)]. *J. Chem. Phys.*, 117:3526–3527, 2002.
- [32] M. Kawata and U. Nagashima. Particle mesh Ewald method for three-dimensional systems with two-dimensional periodicity. *Chem. Phys. Lett.*, 340:165–172, 2001.
- [33] P. Koehl. Electrostatics calculations: latest methodological advances. *Curr. Opin. Struct. Biol.*, 16:142–151, 2006.
- [34] J. Kolafa and J. W. Perram. Cutoff errors in the Ewald summation formulas for point-charge systems. *Mol. Simulat.*, 9:351–368, 1992.
- [35] J. Lekner. Summation of dipolar fields in simulated liquid vapor interfaces. *Physica A*, 157:826–838, 1989.
- [36] J. Lekner. Summation of Coulomb fields in computer-simulated disordered-systems. *Physica A*, 176:485–498, 1991.
- [37] D. Lindbo and A.-K. Tornberg. Spectral accuracy in fast Ewald-based methods for particle simulations. Accepted for publication in *J. Comput. Phys.*, 2011.

- [38] M Mazars. Comment on “Rapid calculation of the Coulomb component of the stress tensor for three-dimensional systems with two-dimensional periodicity” [J. Chem. Phys. 115, 4457 (2001)]. *J. Chem. Phys.*, 117:3524–3525, 2002.
- [39] M. Mazars. Lekner summations and Ewald summations for quasi-two-dimensional systems. *Mol. Phys.*, 103:1241–1260, 2005.
- [40] M. Narasimhan and M. Karthikeyan. Evaluation of Fourier transform integrals using FFT with improved accuracy and its applications. *IEEE T. Antenn. Propag.*, 32:404–408, 1984.
- [41] A. Neelov, S. A. Ghasemi, and S. Goedecker. Particle-particle, particle-scaling function algorithm for electrostatic problems in free boundary conditions. *J. Chem. Phys.*, 127, 2007.
- [42] D. E. Parry. The electrostatic potential in the surface region of an ionic crystal. *Surf. Sci.*, 49:433–440, 1975.
- [43] D. E. Parry. Errata; The electrostatic potential in the surface region of an ionic crystal. *Surf. Sci.*, 54:195–195, 1976.
- [44] M. A. Pinsky. *Introduction to Fourier Analysis and Wavelets (Graduate Studies in Mathematics)*. American Mathematical Society, 2009.
- [45] W. H. Press, S. A. Teukolsky, W. T. Vetterling, and B. P. Flannery. *Numerical Recipes 3rd Edition: The Art of Scientific Computing*. Cambridge University Press, 2007.
- [46] Y. J. Rhee, J. W. Halley, J. Hautman, and A. Rahman. Ewald methods in molecular-dynamics for systems of finite extent in one of 3 dimensions. *Phys. Rev. B*, 40:36–42, 1989.
- [47] T. J. Rivlin. *Chebyshev Polynomials: From Approximation Theory to Algebra and Number Theory*. Wiley-Interscience, 2 edition, 1990.
- [48] T. J. Rivlin. *An Introduction to the Approximation of Functions*. Dover Publications, 2010.
- [49] Y. B. Shan, J. L. Klepeis, M. P. Eastwood, R. O. Dror, and D. E. Shaw. Gaussian split Ewald: A fast Ewald mesh method for molecular simulation. *J. Chem. Phys.*, 122, 2005.
- [50] E. Spohr. Effect of electrostatic boundary conditions and system size on the interfacial properties of water and aqueous solutions. *J. Chem. Phys.*, 107:6342–6348, 1997.
- [51] J. Strain. Fast potential-theory .2. layer potentials and discrete sums. *J. Comp. Phys.*, 99:251–270, 1992.
- [52] O. Takemoto, T. Ohyama, and A. Tohsaki. Direct sum of Coulomb potential without ambiguities of conditionally convergent series. *Prog. Theor. Phys.*, 109(4):563–573, 2003.
- [53] A. Vretblad. *Fourier Analysis and Its Applications*. Springer, 2003.
- [54] I. C. Yeh and M. L. Berkowitz. Ewald summation for systems with slab geometry. *J. Chem. Phys.*, 111:3155–3162, 1999.

- [55] D. Zwillinger, editor. *Table of Integrals, Series, and Products, Seventh Edition*. Academic Press, 2007.